Available online at www.sciencedirect.com
SCIENCE DIRECT®
Polyhedron 24 (2005) 823–830
POLYHEDRON
www.elsevier.com/locate/poly

Synthesis and characterization of new polynuclear lanthanide coordination polymers with 4,4′-oxybis(benzoic acid)

Yi-Bo Wang [a], Chang-Yan Sun [a], Xiang-Jun Zheng [a], Song Gao [b], Shao-Zhe Lu [c], Lin-Pei Jin [a,*]

[a] *Department of Chemistry, Beijing Normal University, Xinjiekou Road, Beijing 100875, PR China*
[b] *State Key Laboratory of Rare Earth Materials Chemistry and Applications, College of Chemistry and molecular Engineering, Peking University, Beijing, 100871, PR China*
[c] *Laboratory of Excited States Processes, Chinese Academy of Sciences; Changchun Institute of Optics, Fine Mechanics and Physics, Chinese Academy of Sciences, Changchun 130021, PR China*

Received 8 December 2004; accepted 22 February 2005
Available online 14 April 2005

Abstract

Three new polynuclear lanthanide coordination polymers $[Ln_5(\mu_3\text{-}OH)(oba)_7(H_2O)_2]_n \cdot 0.5nH_2O$ (Ln = Eu (**1**), Ho (**2**)) and $[Yb_6(oba)_9(H_2O)]_n$ (**3**) (H_2oba = 4,4′-oxybis(benzoic acid)), were prepared by hydrothermal reactions. **1** and **2** are isomorphous and exhibit complicated three-dimensional structures based on $[Ln_5(\mu_3\text{-}OH)(oba)_7(H_2O)_2]$ building blocks. In the asymmetric unit, there are five different coordination environments of Ln(III) ions, including a trinuclear hydroxo core. Complex **3** is a three-dimensional coordination polymer built up from a hexanuclear building block. In **3**, Yb(III) ions have six different chemical environments and are in a regular arrangement, resulting in pseudohexagonal prisms along the *a*-axis. The luminescent property of **1** and magnetic behaviors of **2** and **3** have also been studied.

Keywords: Polynuclear; Coordination polymer; Lanthanide; Magnetic susceptibility; Photophysical property

1. Introduction

Coordination polymers have been extensively studied recently due to their interesting structures coupled with their promising applications in ion and solvent molecule exchanges [1–5], gas sorption [6–10], luminescence [11,12], magnetism [13,14] and catalytic behavior [15–17]. While much current research has focused on transition metal coordination polymers [18–27], lanthanide coordination polymers, particularly polynuclear systems, have received less attention owing to the high coordination number and the variable coordination environments of the lanthanides. However, the introduction of polynuclear lanthanide species into the skeleton may create unusual architectures, and polynuclear lanthanide complexes may also exhibit promising magnetic and luminescence properties as a consequence of the unique spectroscopic and electronic characteristics associated with their $4f^n$ electronic configuration. Only a few examples of polynuclear lanthanide coordination polymers have been prepared by lanthanide hydrolysis controlled by different supporting ligands [28–31]. The cubane-like tetranuclear $[Ln_4(\mu_3\text{-}OH)_4]^{8+}$ unit is a common structural motif in these complexes [29–31]. Here, we report pentanuclear lanthanide coordination polymers $[Ln_5(\mu_3\text{-}OH)(oba)_7(H_2O)_2]_n \cdot 0.5nH_2O$ (Ln = Eu (**1**), Ho (**2**)), in which both hydroxyl and carboxyl groups link the lanthanide (III) ions into building

* Corresponding author. Tel.: +01058805522/861062205522; fax: +8601058802075/861062202075.
E-mail address: lpjin@bnu.edu.cn (L.-P. Jin).

0277-5387/$ - see front matter © 2005 Elsevier Ltd. All rights reserved.
doi:10.1016/j.poly.2005.02.022

blocks, and a hexanuclear ytterbium coordination polymer $[Yb_6(oba)_9(H_2O)]_n$ (**3**).

2. Experimental

2.1. Chemicals and measurements

$EuCl_3 \cdot 6H_2O$, $HoCl_3 \cdot 6H_2O$ and $YbCl_3 \cdot 6H_2O$ were prepared by dissolving their oxides in concentrated hydrochloric acid, respectively, and the solvents were evaporated to dryness. The lanthanide and water contents of the lanthanide chloride hydrates were determined by EDTA titration. All the other reagents were commercially available and used without further purification. Elemental analyses were performed on an Elementar Vario EL analyzer. The IR spectra were recorded with a Nicolet Avatar 360 FT-IR spectrometer using the KBr pellet technique. The luminescence spectra were recorded at 77 K using a YAG:Nd laser with an excitation wavelength of 355 nm and a SPEX 1403 double grating monochromator. The temperature dependence of magnetic susceptibility for crystalline samples was recorded on an Oxford MagLab 2000 magnetometer in the temperature range of 2–300 K.

2.2. Synthesis

*$[Eu_5(oba)_7(OH)(H_2O)_2]_n \cdot 0.5n(H_2O)$ (**1**)*. A mixture of $EuCl_3 \cdot 6H_2O$ (0.037 g, 0.1 mmol), H_2oba (0.039 g, 0.15 mmol), H_2O (10 ml) and 0.65 M NaOH aqueous solution (0.31 ml, 0.20 mmol) was sealed in a 23-ml stainless-steel reactor with a Teflon liner and heated at 200 °C for 72 h, then slowly cooled to room temperature. Colorless crystals of **1** were obtained. Yield: 0.02 g (38.4%). *Anal*. Calc. for $C_{98}H_{62}Eu_5O_{38.50}$: C, 45.00; H, 2.37; Found: C, 44.89; H, 2.32%. IR (KBr, cm^{-1}): 3447m, 1598s, 1524s, 1400s, 1253s, 1233s, 1160s, 1012w, 881m, 784s, 656w.

*$[Ho_5(oba)_7(OH)(H_2O)_2]_n \cdot 0.5nH_2O$ (**2**)*. Light yellow crystals of **2** were prepared in the same manner as above. Yield: 0.017 g (31.9%). *Anal*. Calc. for $C_{98}H_{62}Ho_5O_{38.50}$: C, 43.91; H, 2.11; Found: C, 44.05; H, 2.30%. IR (KBr, cm^{-1}): 3459m, 1599s, 1526s, 1414s, 1254s, 1235s, 1161s, 1012w, 882m, 784s, 658m.

*$[Yb_6(oba)_9(H_2O)]_n$ (**3**)*. Colorless crystals of **3** were obtained in the same manner. Yield: 0.048 g (43.5%). *Anal*. Calc. for $C_{126}H_{74}O_{46}Yb_6$: C, 45.01; H, 2.16; Found: C, 44.99; H, 2.24%. IR (KBr, cm^{-1}): 3439m, 1599s, 1533s, 1417s, 1305m, 1252s, 1161s, 1097m, 1012w, 881m, 783s, 656w.

2.3. X-ray diffraction determination

The X-ray single crystal data collections for complexes **1**–**3** were performed on a Bruker Smart 1000 CCD diffractometer, using graphite-monochromated Mo Kα radiation ($\lambda = 0.71073$ Å). Semi-empirical absorption corrections were applied using the SADABS program. The structures were solved by direct methods and refined by full-matrix least square on F^2 using the SHELXTL-97 program [32]. All non-hydrogen atoms were refined anisotropically. The hydrogen atoms were generated geometrically and treated by a mixture of independent and constrained refinement. The crystallographic data for complexes **1**–**3** are listed in Table 1, and selected bond lengths (Å) in Table 2.

Table 1
Crystal data for **1**–**3**

Compound	**1**	**2**	**3**
Empirical formula	$C_{98}H_{62}Eu_5O_{38.50}$	$C_{98}H_{62}Ho_5O_{38.50}$	$C_{126}H_{74}O_{46}Yb_6$
Formula weight	2615.28	2680.13	3360.08
Crystal system	monoclinic	monoclinic	monoclinic
Space group	*P*2(1)/*c*	*P*2(1)/*c*	*Pc*
a (Å)	27.983(7)	27.947(9)	14.657(4)
b (Å)	20.538(5)	20.367(6)	23.113(7)
c (Å)	15.833(4)	15.730(5)	20.187(5)
α (°)	90	90	90
β (°)	90.736(5)	90.572(5)	115.408(16)
γ (°)	90	90	90
Z	4	4	2
V (Å^3)	9099(4)	8953(5)	6177(3)
ρ_{calcd} (g cm^{-3})	1.909	1.988	1.806
Temperature (K)	293(2)	293(2)	293(2)
μ (mm^{-1})	3.491	4.464	4.584
Reflections collected	26254, 12718	48535, 18197	31616, 19620
Total, independent, R_{int}	0.1724	0.0651	0.0536
λ (Mo Kα), (Å)	0.71073	0.71073	0.71073
R_1, wR_2 [$I > 2\sigma(I)$]	0.0560, 0.0742	0.0504, 0.1105	0.0611, 0.1343

Table 2
Selected bond lengths (Å) for **1**–**3**

1					
Eu(1)–O(1)	2.68(1)	Eu(2)–O(35)#1	2.28(2)	Eu(4)–O(20)	2.71(1)
Eu(1)–O(2)	2.42(1)	Eu(2)–O(37)	2.43(1)	Eu(4)–O(24)	2.33(1)
Eu(1)–O(6)#3	2.45(1)	Eu(2)–O(38)	2.48(1)	Eu(4)–O(26)#7	2.41(1)
Eu(1)–O(11)	2.48(2)	Eu(3)–O(7)	2.53(1)	Eu(4)–O(29)#3	2.49(1)
Eu(1)–O(15)#2	2.43(1)	Eu(3)–O(12)	2.33(2)	Eu(4)–O(31)#3	2.42(1)
Eu(1)–O(17)#1	2.36(2)	Eu(3)–O(14)#2	2.29(1)	Eu(5)–O(5)	2.39(1)
Eu(1)–O(34)#1	2.47(2)	Eu(3)–O(21)#4	2.26(1)	Eu(5)–O(9)	2.27(1)
Eu(1)–O(38)	2.36(1)	Eu(3)–O(27)#6	2.33(1)	Eu(5)–O(20)	2.36(1)
Eu(2)–O(1)	2.39(1)	Eu(3)–O(36)	2.42(1)	Eu(5)–O(25)	2.32(1)
Eu(2)–O(6)	2.58(1)	Eu(3)–O(38)	2.36(1)	Eu(5)–O(29)	2.53(1)
Eu(2)–O(7)	2.49(1)	Eu(4)–O(4)	2.30(1)	Eu(5)–O(30)	2.44(1)
Eu(2)–O(16)#4	2.40(1)	Eu(4)–O(10)#3	2.37(1)	Eu(5)–O(31)	2.61(1)
Eu(2)–O(22)#4	2.35(1)	Eu(4)–O(19)	2.43(1)	Eu(5)–O(32)	2.43(1)

Symmetry operation: #1 $x + 1$, $-y + 1/2$, $z - 1/2$; #2 $-x$, $-y + 1$, $-z - 1$; #3 x, $-y + 1/2$, $z - 1/2$; #4 $x + 1$, y, z; #5 x, $-y + 1/2$, $z + 1/2$; #6 $-x$, $y + 1/2$, $-z + 1/2$; #7 x, y, $z - 1$.

2					
Ho(1)–O(1)	2.76(1)	Ho(2)–O(35)#1	2.20(1)	Ho(4)–O(20)	2.71(1)
Ho(1)–O(2)	2.35(1)	Ho(2)–O(37)	2.39(1)	Ho(4)–O(24)	2.28(1)
Ho(1)–O(6)#3	2.40(1)	Ho(2)–O(38)	2.42(1)	Ho(4)–O(26)#6	2.36(1)
Ho(1)–O(11)	2.40(1)	Ho(3)–O(7)	2.55(1)	Ho(4)–O(29)#3	2.46(1)
Ho(1)–O(15)#2	2.33(1)	Ho(3)–O(12)	2.28(1)	Ho(4)–O(31)#3	2.36(1)
Ho(1)–O(17)#1	2.31(1)	Ho(3)–O(14)#2	2.26(1)	Ho(5)–O(5)	2.33(1)
Ho(1)–O(34)#1	2.37(1)	Ho(3)–O(21)#4	2.24(1)	Ho(5)–O(9)	2.26(1)
Ho(1)–O(38)	2.33(1)	Ho(3)–O(27)#5	2.27(1)	Ho(5)–O(20)	2.32(1)
Ho(2)–O(1)	2.32(1)	Ho(3)–O(36)	2.35(1)	Ho(5)–O(25)	2.25(1)
Ho(2)–O(6)	2.54(1)	Ho(3)–O(38)	2.32(1)	Ho(5)–O(29)	2.48(1)
Ho(2)–O(7)	2.43(1)	Ho(4)–O(4)	2.25(1)	Ho(5)–O(30)	2.37(1)
Ho(2)–O(16)#4	2.32(1)	Ho(4)–O(10)#3	2.30(1)	Ho(5)–O(31)	2.62(1)
Ho(2)–O(22)#4	2.31(1)	Ho(4)–O(19)	2.37(1)	Ho(5)–O(32)	2.37(1)

Symmetry operation: #1 $x + 1$, $-y + 1/2$, $z - 1/2$; #2 $-x + 2$, $-y + 1$, $-z + 1$; #3 x, $-y + 1/2$, $z - 1/2$; #4 $x + 1$, y, z; #5 $-x + 2$, $y + 1/2$, $-z + 5/2$; #6 x, y, $z - 1$.

3					
Yb(1)–O(2)	2.23(3)	Yb(3)–O(15)	2.31(2)	Yb(5)–O(12)	2.23(2)
Yb(1)–O(7)	2.24(2)	Yb(3)–O(21)	2.47(2)	Yb(5)–O(35)#4	2.23(2)
Yb(1)–O(10)#1	2.25(2)	Yb(3)–O(22)	2.34(2)	Yb(5)–O(37)#5	2.20(2)
Yb(1)–O(11)	2.22(2)	Yb(3)–O(25)#2	2.15(2)	Yb(5)–O(39)	2.51(4)
Yb(1)–O(42)#1	2.26(2)	Yb(3)–O(26)	2.23(2)	Yb(5)–O(40)	2.27(3)
Yb(1)–O(45)	2.30(4)	Yb(3)–O(30)#4	2.25(2)	Yb(5)–O(41)#1	2.33(2)
Yb(2)–O(4)#3	2.59(2)	Yb(3)–O(31)	2.20(2)	Yb(5)–O(42)#1	2.60(2)
Yb(2)–O(5)#3	2.33(2)	Yb(4)–O(1)#6	2.29(4)	Yb(5)–O(44)	2.26(4)
Yb(2)–O(14)	2.30(2)	Yb(4)–O(6)#6	2.25(2)	Yb(6)–O(4)#6	2.31(2)
Yb(2)–O(15)	2.58(2)	Yb(4)–O(7)#6	2.60(2)	Yb(6)–O(17)#7	2.22(2)
Yb(2)–O(16)	2.25(2)	Yb(4)–O(9)#5	2.20(1)	Yb(6)–O(19)#8	2.22(2)
Yb(2)–O(20)#2	2.20(2)	Yb(4)–O(27)	2.26(2)	Yb(6)–O(34)#4	2.21(2)
Yb(2)–O(21)	2.32(2)	Yb(4)–O(29)#4	2.15(2)	Yb(6)–O(36)#5	2.20(2)
Yb(2)–O(24)#2	2.29(2)	Yb(4)–O(32)	2.28(2)	Yb(6)–O(47)	2.22(2)

Symmetry operation: #1 $x - 1$, $-y + 1$, $z - 1/2$; #2 $x - 1$, $-y$, $z - 1/2$; #3 x, $y - 1$, $z + 1$; #4 $x + 1$, y, z; #5 $x - 1$, y, z; #6 x, $-y + 1$, $z + 1/2$; #7 x, $-y$, $z - 1/2$; #8 $x - 1$, y, $z - 1$.

3. Results and discussion

3.1. Description of the structures

In complexes **1**–**3**, the carboxyl groups of the H_2oba ligands are all deprotonated and adopt four kinds of coordination modes (see Scheme 1). **1** and **2** are isomorphous and thus only the structures of **1** and **3** will be discussed here.

*$[Eu_5(oba)_7(OH)(H_2O)_2]_n \cdot 0.5nH_2O$ (**1**)*. Complex **1** is a three-dimensional polymer containing rugby-like channels. Three types of coordination modes of oba^{2-} ligands are present in the structure: (a) one carboxylate group of the oba^{2-} ligand adopts a bridging bidentate

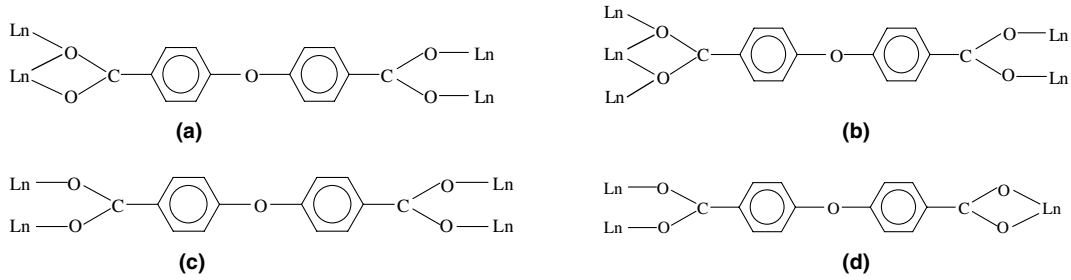

Scheme 1. The coordination modes of oba^{2-} ligands in **1**–**3**.

mode, while the other adopts a chelating-bridging tridentate mode, connecting four Eu(III) ions ($^{a}oba^{2-}$, Scheme 1(a)); (b) one carboxylate group of the oba^{2-} ligand adopts a bridging bidentate mode, while the other adopts a chelating-bridging tetradentate mode, connecting five Eu(III) ions ($^{b}oba^{2-}$, Scheme 1(b)); (c) each carboxylate group of the oba^{2-} ligand adopts a bridging bidentate mode, connecting four Eu(III) ions ($^{c}oba^{2-}$, Scheme 1(c)). The asymmetric unit of **1** consists of five Eu(III) ions, seven oba^{2-} ligands, one hydroxyl group, two coordinated water molecules and half a lattice water molecule. The coordination environments of five Eu(III) ions are shown in Fig. 1(a) and the details are listed in Table 3. For clarity, we may divide the coordination environments into two parts (Fig. 1(b) and (c)), which are connected by one $^{a}oba^{2-}$ and two $^{b}oba^{2-}$ ligands. In Fig. 1(b), Eu1, Eu2 and Eu3 are linked together by one μ_3-OH, and therefore a distorted tetrahedron is formed by three Eu^{3+} ions and one oxygen atom of μ_3-OH, where the distance of the oxygen atom of

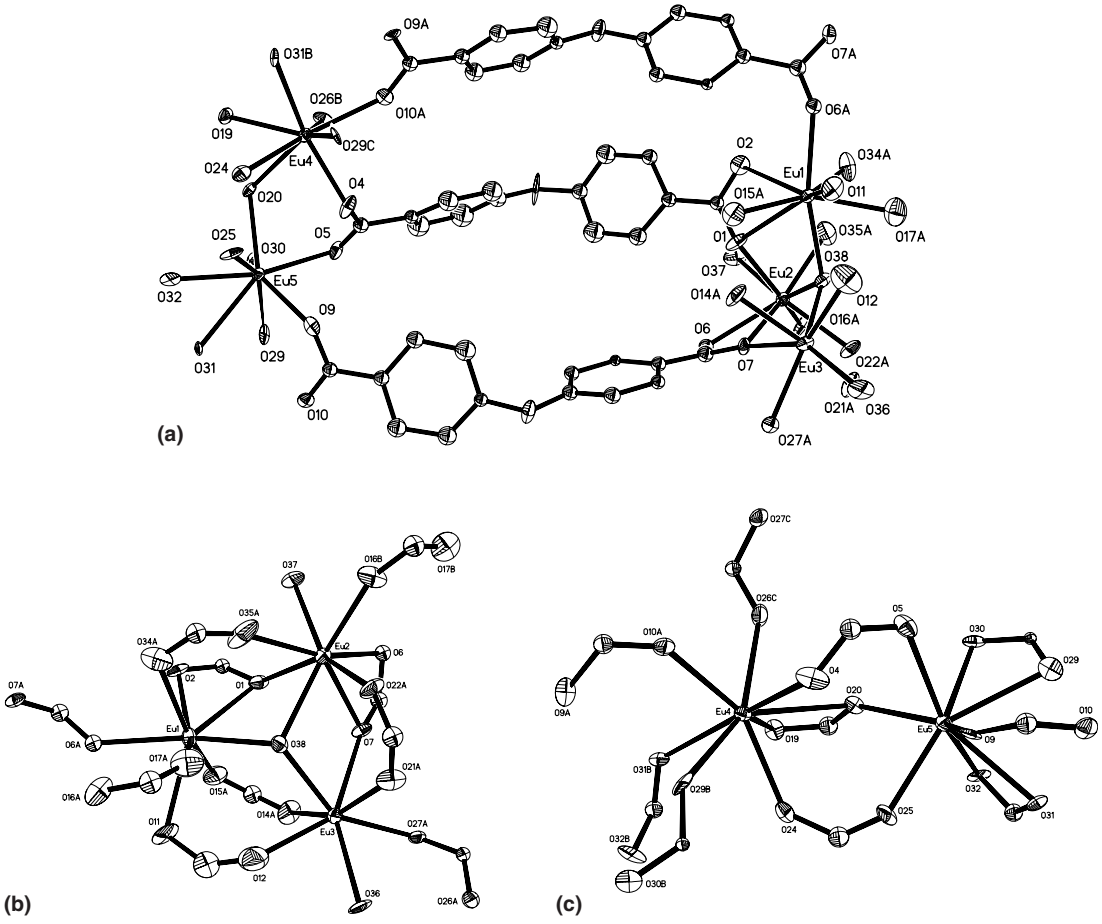

Fig. 1. (a) The coordination environment of Eu^{3+} ions in **1**; (b) The coordination environment of Eu^{3+} ions of the trinuclear core; (c) The coordination environment of the other two Eu^{3+} ions in **1** with thermal ellipsoids at 20% probability. All hydrogen atoms and partial carbon atoms are omitted for clarity.

Table 3
The coordination environment of Eu^{3+} in **1**

Metal atom	CN	No. of Coordinated μ_3-OH	No. of coordinated carboxyl oxygen atoms			No. of coordinated H_2O
			$^{a}oba^{2-}$	$^{b}oba^{2-}$	$^{c}oba^{2-}$	
Eu1	8	1	4	1	2	
Eu2	8	1	3	2	1	1
Eu3	7	1	1	1	3	1
Eu4	8		6	1	1	
Eu5	8		6	1	1	

CN, coordination number; No, number.

μ_3-OH to the triangular metal face is 0.639Å. In the europium hydroxo core, the separations of Eu1···Eu2, Eu2···Eu3 and Eu1···Eu3 are 3.898, 3.977 and 4.119 Å, respectively, and a pair of adjacent Eu^{3+} ions are bridged by two carboxylate groups of two oba^{2-} ligands through bridging bidentate and chelating-bridging tridentate fashion. Thus the europium hydroxo core is surrounded by the six carboxyl groups and a cage-like structure is produced. In the trinuclear core, the average distances of Eu1–O(COO^-), Eu2–O(COO^-), Eu3–O(COO^-) and Eu–O(OH^-) are 2.470, 2.416, 2.347 and 2.400 Å, respectively, which are in accord with the values in $[Eu_{15}(\mu_3\text{-}OH)_{20}(\mu_5\text{-}X)]^{24+}$ [33]. The other two Eu^{3+} ions (Fig. 1(c)), Eu4 and Eu5, are bridged by three carboxyl groups of three oba^{2-} ligands through bridging bidentate and chelating-bridging tridentate coordination modes. The average distances of Eu4–O(COO^-) and Eu5–O(COO^-) are 2.430 and 2.418 Å, which are in agreement with the common distances of Eu–O(COO^-), and the distance of Eu4···Eu5 is 4.281 Å. The Eu(III) ions along the *a*-axis are bridged by $^{a}oba^{2-}$ and $^{b}oba^{2-}$ ligands into one-dimensional double-chains with rugby-like micropores. These chains are further cross-linked by oba^{2-} ligands, resulting in the formation of a three-dimensional network, as shown in Fig. 2. There are small rugby-like channels along the *c*-axis.

*$[Yb_6(oba)_9(H_2O)]_n$ (**3**)*. Complex **3** is a three-dimensional polymer. The hexanuclear species $[Yb_6(oba)_9(H_2O)]$ may be viewed as the building block. There are three types of coordination modes of oba^{2-} ligands in **3**: (a) one carboxylate group of the oba^{2-} ligand adopts a bridging bidentate mode, while the other adopts a chelating-bridging tridentate mode, connecting four Yb(III) ions ($^{a}oba^{2-}$, Scheme 1(a)); (b) each carboxylate group of the oba^{2-} ligand adopts a bridging bidentate mode, connecting four Yb(III) ions ($^{c}oba^{2-}$, Scheme 1(c)); (c) one carboxylate group of the oba^{2-} ligand adopts a bridging bidentate mode, while the other adopts a chelating bidentate mode, connecting three Yb(III) ions ($^{d}oba^{2-}$, Scheme 1(d)). In the asymmetrical unit of **3**, there are six Yb(III) ions, nine oba^{2-} ligands and one aqua ligand. The coordination environment of Yb(III) ions is shown in Fig. 3 and the details are listed in Table 4. For clarity we can also divide the Yb(III) ions into two parts: part 1 consists of Yb1, Yb5 and Yb6; while part 2 consists of Yb2, Yb3 and Yb4. The two parts are linked by two $^{a}oba^{2-}$ ligands. In part 1, Yb5 and Yb6 are connected by two bridging bidentate carboxyl groups of two oba^{2-} ligands; while Yb5 and Yb1 are connected by two bridging bidentate carboxylate groups and one chelating-bridging tridentate carboxyl group of three oba^{2-} ligands. In part 2, Yb3 is connected to Yb4 by three bridging bidentate carboxyl groups of three oba^{2-} ligands, and connected to Yb2 by two chelating-bridging tridentate carboxyl groups and one bridging bidentate carboxylate group of three oba^{2-} ligands. The average distances of Yb–O(COO^-)

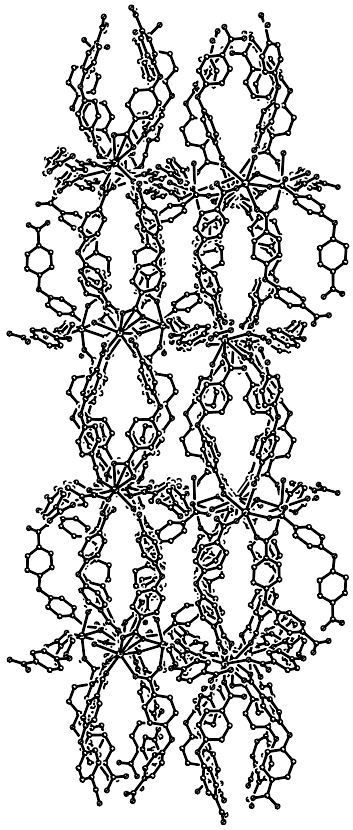

Fig. 2. The three-dimensional network of **1** viewed along the *c*-axis.

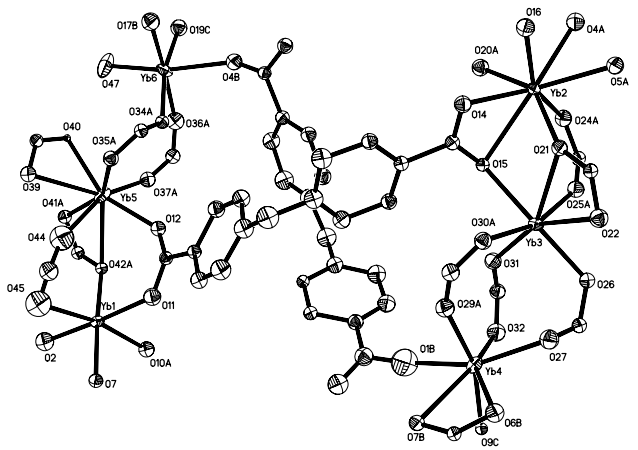

Fig. 3. The coordination environment of Yb^{3+} ions in **3** with thermal ellipsoids at 20% probability. All hydrogen atoms are omitted for clarity.

Table 4
The coordination environment of Yb^{3+} in **3**

	CN	No. of carboxyl oxygen atoms			No. of coordinated H_2O
		$^{a}oba^{2-}$	$^{c}oba^{2-}$	$^{d}oba^{2-}$	
Yb1	6	6			
Yb2	8	6	2		
Yb3	7	4	3		
Yb4	7	4	3		
Yb5	8	4	1	3	
Yb6	6	1	3	1	1

CN, coordination number; No, number.

(from Yb1 to Yb6) are 2.249, 2.356, 2.280, 2.290, 2.330 and 2.231 Å, respectively, and the separations of Yb1···Yb5, Yb5···Yb6, Yb2···Yb3 and Yb3···Yb4 are 4.002, 4.510, 3.823 and 4.330 Å, respectively.

In each asymmetrical unit of **3**, six Yb(III) ions are arranged in the form of a non-planar six-member ring. And along the *a*-axis, two adjacent six-member rings are parallel to each other. As shown in Fig. 4, for instance, a six-member ring constructed by Yb2J, Yb3J, Yb4J, Yb1J, Yb5J and Yb6J is parallel to an adjacent six-member ring formed by Yb2M, Yb3M, Yb4M, Yb1M Yb5M and Yb6M. These two rings are pillared by oba^{2-} ligands along the *a*-axis to yield a pseudohexagonal prism, which is the first example of such an array of lanthanide (III) ions. These pseudoprisms are cross-linked by oba^{2-} ligands, resulting in the formation of a three-dimensional network.

Comparing the structures of **1**–**3**, it can be seen that oba^{2-} ligands display different coordination modes. In **1** and **2**, there are three kinds of oba^{2-} ligands: $^{a}oba^{2-}$, $^{b}oba^{2-}$ and $^{c}oba^{2-}$; while in **3**, the three kinds of oba^{2-} ligands are $^{a}oba^{2-}$, $^{c}oba^{2-}$ and $^{d}oba^{2-}$. The different coordination modes of oba^{2-} ligands lead to the different structures.

Although the "O" atoms between two benzene rings in each oba^{2-} ligand do not participate in the coordination to Ln(III) ions, however, they are important in the structure. With the presence of these "O" atoms, oba^{2-} ligands act as V-shaped, not linear ligands. It is the V-shaped configuration of oba^{2-} ligands, which facilitates the benzene rings and carboxylate groups to adjust their steric configurations more freely and allow the oba^{2-} ligands to display a variety of coordination modes.

3.2. Photophysical properties of complex *1*

The room temperature spectra of powders for **1** are less developed, we comment about low temperature spectra only. The high-resolution emission spectrum of **1** corresponding to $^{5}D_0 \rightarrow {}^{7}F_J$ ($J = 0$–4) transitions excited by 355 nm at 77 K is shown in Fig. 5. The most intensive transition is $^{5}D_0 \rightarrow {}^{7}F_2$, which implies red emission light of **1**. The number of components of the $^{5}D_0 \rightarrow {}^{7}F_1$ transition indicates the presence of more than one chemically different Eu(III) ions site [34]. The intensity of the $^{5}D_0 \rightarrow {}^{7}F_0$ transition is relatively weak and the emission band is broad (see the inserted spectrum in Fig. 5). The inhomogeneous broadening of the $^{5}D_0 \rightarrow {}^{7}F_0$ emission band arises from the site to site variation of the local field acting on the ions, and has consequently been studied by selective excitation techniques.

Setting the analyzing wavenumber to 16233 cm^{-1} and scanning in the range of 578.72–580.4 nm ($^{7}F_0 \rightarrow {}^{5}D_0$), the excitation spectrum (Fig. 6) was obtained. There are two obvious groups of peaks located at about 579.4 and 580.0 nm. The negative charges on the ligands around Eu1, Eu2, Eu3, Eu4 and Eu5 are approximately 3.4, 2.5, 2.6, 3.3 and 3.2, respectively. They can be divided into two groups. One group (3.4, 3.3 and 3.2) contains Eu1, Eu4 and Eu5. The other group (2.5 and 2.6) contains Eu2 and Eu3. As is known, the peak position of $^{7}F_0 \rightarrow {}^{5}D_0$ will shift to lower energy with increasing negative charge on the ligands [35]. So the left peak denoted as A in Fig. 6 can be ascribed to the contribution of $^{5}D_0$ levels of Eu2 and Eu3, and the right peak denoted as B in Fig. 6 can be ascribed to the contribution of $^{5}D_0$ levels of Eu1, Eu4 and Eu5.

3.3. Magnetic properties

The temperature dependence of the magnetic susceptibility of **2** was measured in the temperature range 2–300 K (Fig. 7). The magnetic susceptibility above 50 K obeys the Curie–Weiss law [$\chi = C/(T - \theta)$] with $C = 71.43$ cm^3 mol^{-1} K and $\theta = -10.79$ K. The C value is close to the expected value of 70.35 cm^3 mol^{-1} K for five non-interacting Ho^{3+} free ions. The continuous

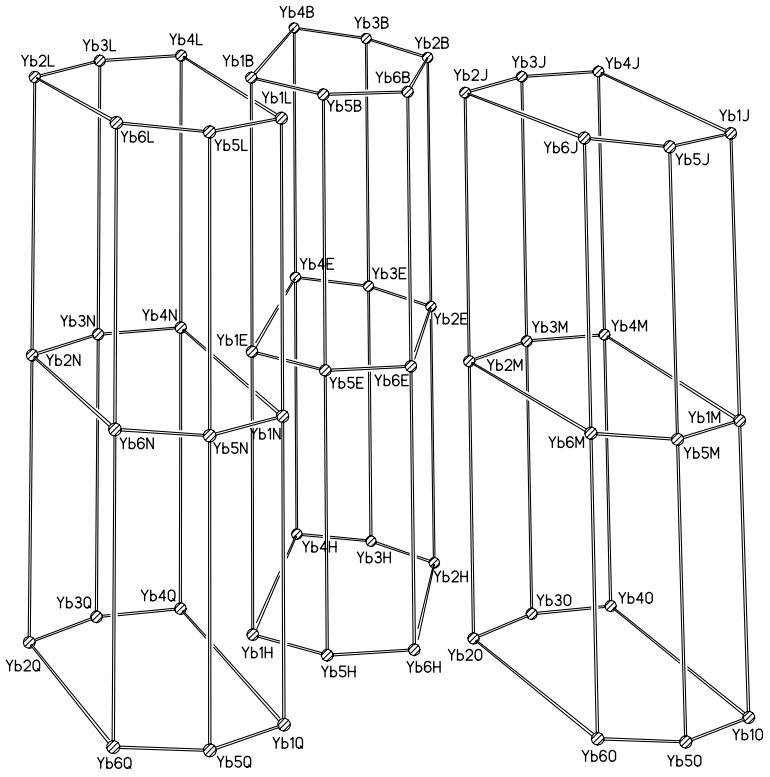

Fig. 4. The hexagonal pseudoprism distribution of Yb(III) ions in **3**.

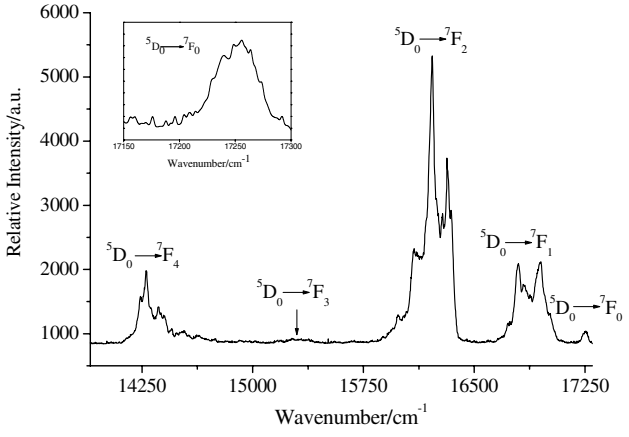

Fig. 5. Emission spectrum of **1** corresponding to $^5D_0 \rightarrow {}^7F_J$ (J = 0–4) transitions at 77 K, λ_{exc} = 355 nm.

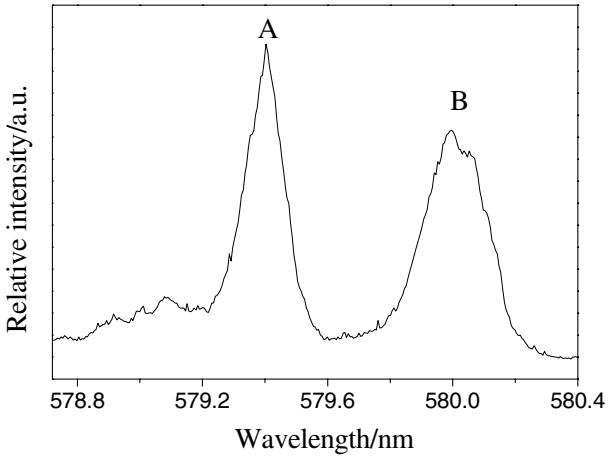

Fig. 6. $^7F_0 \rightarrow {}^5D_0$ excitatation spectrum of powders for **1** recorded at 77 K, λ_m = 616 nm.

decrease in $\chi_M T$ upon cooling should be mainly attributed to the crystal field splitting of a single Ho^{3+} ion together with the possible contribution of the weak interaction through oxygen atoms of hydroxyl and carboxylate bridge with 3.910–4.043 Å Ho···Ho distances.

The variable-temperature magnetic susceptibility of **3** is displayed in Fig. 8, where χ_M is the corrected molar magnetic susceptibility per [Yb_6] unit. At room temperature, the value of $\chi_M T$ is 13.41 $cm^3\,mol^{-1}\,K$, which is approximately close to the calculated value for six Yb free ions (15.42 $cm^3\,mol^{-1}\,K$). Upon cooling, $\chi_M T$ decreases steadily and fast at low temperatures. These results primarily arise from the splitting of the ligand field of the Yb(III) ion together with the possible contribution of the weak antiferromagnetic coupling between Yb(III) ions, considering a possible interaction through two carboxylate bridges with 3.823–4.510 Å Yb···Yb distances. The magnetic susceptibility above 100 K obeys the Curie–Weiss law with the Weiss constant $\theta = -42.61$ K and the Curie constant $C = 15.43$ $cm^3\,mol^{-1}\,K$.

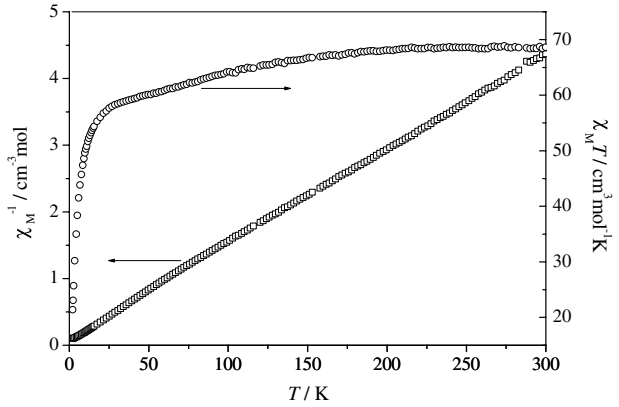

Fig. 7. Plot of the temperature dependence of $\chi_M T$ (○) and χ_M^{-1} (□) for **2** (per $[Ho]_5$ unit).

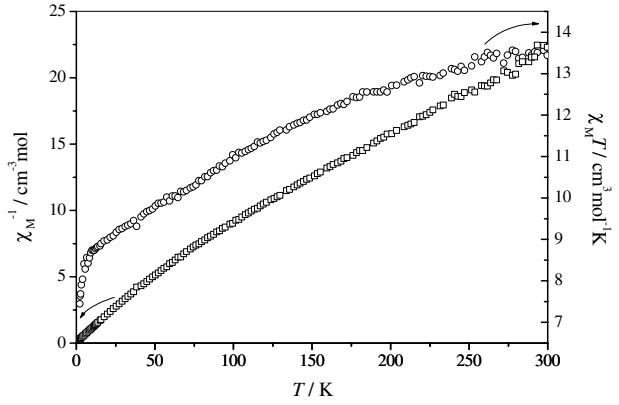

Fig. 8. Plot of the temperature dependence of $\chi_M T$ (○) and χ_M^{-1} (□) for **3** (per $[Yb]_6$ unit).

4. Supplementary material

Crystallographic data for the structural analysis have been deposited with the Cambridge Crystallographic Data Centre, CCDC Nos. 250474, 250475 and 250476 for **1**–**3**, respectively. Copies of this information may be obtained free of charge from the CCDC, 12 Union Road, Cambridge, CB2 1EZ, UK (fax: +44-1223-336-033; e-mail: deposit@ccdc.cam.ac.uk or www: http://www.ccdc.cam.ac.uk).

Acknowledgements

This work was supported by National Natural Science Foundation of China (20331010).

References

[1] B.F. Hoskins, R. Robson, J. Am. Chem. Soc 111 (1989) 5962.
[2] B.F. Hoskins, R. Robson, J. Am. Chem. Soc. 112 (1990) 1546.
[3] O.M. Yaghi, H. Li, J. Am. Chem. Soc. 117 (1995) 10401.
[4] G.B. Gardner, D. Venkataraman, J.S. Moore, S. Lee, Nature 374 (1995) 792.
[5] B.F. Abrahams, P.A. Jackson, R. Robson, Angew. Chem. Int. Ed. 37 (1998) 2656.
[6] O.M. Yaghi, G. Li, H. Li, Nature 378 (1995) 703.
[7] D. Venhataraman, G.B. Gardner, S. Lee, J.S. Moore, J. Am. Chem. Soc. 117 (1995) 11600.
[8] M. Kondo, T. Yoshitomi, K. Seki, H. Matsazaka, S. Kitagawa, Angew. Chem. Int. Ed. 36 (1997) 1725.
[9] O.M. Yaghi, M. O'Keeffe, N.W. Ockwig, H.K. Chae, M. Eddaoudi, J. Kim, Nature 423 (2003) 705.
[10] M. Eddaoudi, J. Kim, N. Rosi, D. Vodak, J. Wachter, M. O'Keeffe, O.M. Yaghi, Science 300 (2003) 1127.
[11] T.M. Reineke, M. Eddaoudi, M. Fehr, D. Kelley, O.M. Yaghi, J. Am. Chem. Soc. 121 (1999) 1651.
[12] B.D. Chandler, A.P. Côtó, D.T. Cramb, J.M. Hill, G.K.H. Shimizu, Chem. Commun. (2002) 1900.
[13] G.J. Halder, C.J. Kepert, B. Moubaraki, K.S. Murray, J.D. Cashion, Science 298 (2002) 1762.
[14] D. Maspoch, D. Ruiz-Molina, K. Wurst, N. Domingo, M. Cavallini, F. Biscarini, J. Tejada, C. Rovira, J. Veciana, Nature Mater. 2 (2003) 190.
[15] M. Fujita, Y.J. Kwon, S. Washizu, K. Ogura, J. Am. Chem. Soc. 116 (1994) 1151.
[16] J.S. Seo, D. Wang, H. Lee, S.I. Jun, J. Oh, Y.J. Jeon, K. Kim, Nature 404 (2000) 982.
[17] O.R. Evans, H.L. Ngo, W. Lin, J. Am. Chem. Soc. 123 (2001) 10395.
[18] S. Kitagawa, M. Munakata, Trends Inorg. Chem. 3 (1993) 437.
[19] M.J. Zaworotko, Chem. Soc. Rev. 23 (1994) 283.
[20] M. Munakata, Adv. Inorg. Chem. 46 (1998) 173.
[21] A.J. Blake, N.R. Champness, P. Hubberstey, W.S. Li, M.A. Withersby, M. Schröder, Coord. Chem. Rev. 183 (1999) 117.
[22] M. Eddaoudi, D.B. Moler, H. Li, B. Chen, T.M. Reineike, M. O'Keeffe, O.M. Yaghi, Acc. Chem. Res. 34 (2001) 319.
[23] A.N. Khlobystov, A.J. Blake, N.R. Champness, D.A. Lemenovskii, A.G. Majouga, N.V. Zyk, M. Schröder, Coord. Chem. Rev. 222 (2001) 155.
[24] B. Moulton, M.J. Zaworotko, Chem. Rev. 101 (2001) 1629.
[25] O.R. Evans, W. Li, Acc. Chem. Res. 35 (2002) 511.
[26] K. Kim, Chem. Soc. Rev. 31 (2002) 96.
[27] S. Kitagawa, S. Kawata, Coord. Chem. Rev. 224 (2002) 11.
[28] C. Serre, N. Stock, T. Bein, G. Férey, Inorg. Chem. 43 (2004) 3159.
[29] R. Wang, H. Liu, M.D. Carducci, T. Jin, C. Zheng, Z. Zheng, Inorg. Chem. 40 (2001) 2743.
[30] B.Q. Ma, D.S. Zhang, S. Gao, T.Z. Jin, C.H. Yan, G.X. Xu, Angew. Chem. Int. Ed. 39 (2000) 3644.
[31] X.J. Zheng, L.P. Jin, S. Gao, Inorg. Chem. 43 (2004) 1600.
[32] G.M. Sheldrick, SHELX-97, PC-version, University of Göttingen, Germany, 1997.
[33] R. Wang, H.D. Selby, H. Liu, M.D. Carducci, T. Jin, Z. Zheng, J.W. Anthis, R.J. Staples, Inorg. Chem. 41 (2002) 278.
[34] J.-C.G. Bünzli, G.R. Choppin, Lanthanide Probes in Life, Chemical and Earth Sciences, Elsevier, Amsterdam, 1989.
[35] M. Albin, W.DeW. Horrocks Jr., Inorg. Chem. 24 (1985) 895.